

Search for Tau Flavour Violation at the LHC

E. Carquin¹, J. Ellis², M.E. Gómez³, S. Lola⁴ and J.Rodriguez-Quintero³

¹ Centre of Subatomic Studies, Technical University Federico Santa María, Valparaíso, Chile

² Theory Division, Physics Department, CERN, CH-1211 Geneva 23, Switzerland

³ Department of Applied Physics, University of Huelva, 21071 Huelva, Spain

⁴ Department of Physics, University of Patras, 26500 Patras, Greece

ABSTRACT

We explore the prospects for searches at the LHC for sparticle decays that violate τ lepton number, in the light of neutrino oscillation data and the seesaw model for neutrino masses and mixing. We analyse the theoretical and phenomenological conditions required for tau flavour violation to be observable in $\chi_2 \rightarrow \chi + \tau^\pm \mu^\mp$ decays, for cosmologically interesting values of the relic neutralino LSP density. We study the relevant supersymmetric parameter space in the context of the Constrained Minimal Supersymmetric Extension of the Standard Model (CMSSM) and in SU(5) extensions of the theory. We pay particular attention to the possible signals from hadronic tau decays, that we analyse using PYTHIA event simulation. We find that a signal for τ flavour-violating χ_2 decays may be observable if the branching ratio exceeds about 10%. This may be compatible with the existing upper limit on $\tau \rightarrow \mu\gamma$ decays if there is mixing between right-handed sleptons, as could be induced in non-minimal SU(5) GUTs.

1 Introduction

Data from both atmospheric [1] and solar [2] neutrinos have confirmed the existence of neutrino oscillations with near-maximal $\nu_\mu - \nu_\tau$ mixing (Super-Kamiokande) and large $\nu_e \rightarrow \nu_\mu$ mixing (SNO). These observations would also imply violation of the corresponding charged-lepton numbers, which would be enhanced in supersymmetric theories and might be observable in low-energy experiments. In fact, charged-lepton-number violating processes could occur at embarrassingly large rates if the soft supersymmetry-breaking masses of the squarks and sleptons were not universal. For this reason, it is often assumed that these masses are equal at the grand-unification scale, as in the constrained minimal supersymmetric extension of the Standard Model (CMSSM).

Even within the minimal supersymmetric version of the seesaw model for neutrino masses, renormalization of the soft supersymmetry-breaking slepton masses would occur while running from the GUT scale to the heavy neutrino mass scales. This would be induced by the Dirac Yukawa couplings of the neutrinos [3], since these cannot, in general, be diagonalised simultaneously with the charged-lepton and the slepton mass matrices. This scenario provides a minimal amount of charged-lepton-flavour violation, which could be further enhanced by GUT interactions and/or non-universal slepton masses at the GUT scale.

Within this framework, many signatures for charged-lepton-flavour violation have been considered [4, 5], including $\mu \rightarrow e\gamma$ decays, $\mu - e$ conversions, $\tau \rightarrow \mu\gamma$ and $\tau \rightarrow e\gamma$ decays. In view of the (near-)maximal mixing observed amongst the corresponding neutrino species, one expects these decays to be relatively large when the soft supersymmetry-breaking masses $M_{1/2}$ and/or m_0 are relatively small. Other charged-lepton-flavour violating possibilities that have been considered are the decays $\chi_2 \rightarrow \chi + e^\pm \mu^\mp$ [6, 7], and $\chi_2 \rightarrow \chi + \mu^\pm \tau^\mp$ [8, 9], where χ is the lightest neutralino, assumed here to be the lightest supersymmetric particle (LSP), and χ_2 is the second-lightest neutralino. It has been argued that these decays might have a rate observable at the LHC for certain choices of the CMSSM parameters [8, 9]. These decays would provide search possibilities that are complementary to searches for the flavour-violating decays of charged leptons, since they may be relevant particularly for regions of the supersymmetric parameter space where rare charged lepton decays and conversions are suppressed.

The answer to the question which decay mode offers better detection prospects at the LHC or at a future linear collider depends on the details of both the theoretical model and the experiment. The decay $\chi_2 \rightarrow \chi + \mu^\pm \tau^\mp$ has an experimental signature that is less distinctive than $\chi_2 \rightarrow \chi + e^\pm \mu^\mp$. However, it may have certain theoretical advantages over the latter mode. This is because $\nu_\tau - \nu_\mu$ mixing is known to be essentially maximal, and the feedthrough into the charged-lepton sector is potentially enhanced by larger Dirac Yukawa couplings and/or lighter singlet-neutrino masses, if neutrino masses exhibit the expected hierarchical pattern. These comments imply that the two lepton-flavour-violating modes are complementary, and both have to be studied. In order to assess the observability of $\chi_2 \rightarrow \chi + \tau^\pm \mu^\mp$, the detailed simulation of signal and background events seems unavoidable.

In previous work [9], we observed that the branching ratio for $\chi_2 \rightarrow \chi + \tau^\pm \mu^\mp$ decay is enhanced

when $m_{\chi_2} > m_{\tilde{\tau}_1} > m_\chi$, where $\tilde{\tau}_1$ is the lighter stau slepton. This occurs in a wedge of the $(M_{1/2}, m_0)$ parameter plane in the CMSSM that is complementary to that explored by $\tau \rightarrow \mu\gamma$. The region of CMSSM parameter space where this enhancement occurs includes the region where $\chi - \tilde{\ell}$ coannihilation suppresses the relic density Ω_χ , keeping it within the range $\Omega_\chi h^2 \sim 0.1$ preferred by astrophysics and cosmology, even if $M_{1/2}$ is comparatively large. The interest of this coannihilation region is supported by experimental constraints on the CMSSM, such as m_h and $b \rightarrow s\gamma$ decay, which disfavour low values of $M_{1/2}$.

In the current paper, we revisit the $\chi_2 \rightarrow \chi + \tau^\pm \mu^\mp$ decay mode and extend previous analyses in the following directions:

- *Theoretical framework:* In [9] we considered generic seesaw mixing within the framework of the CMSSM. Here, we will study how the ratio $\Gamma(\chi_2 \rightarrow \chi + \tau^\pm + \mu^\mp)/\Gamma(\chi_2 \rightarrow \chi + \tau^\pm + \tau^\mp)$ is modified under different theoretical assumptions, and what information a possible signal may provide in this respect. Specifically, in our previous analysis we considered only the dominant effects due to large mixing in the 2-3 sector of the charged-slepton mass matrix. Within this framework, the slepton mixing arises essentially only from the LL sector, and large LFV effects may be observed mostly at low $\tan\beta$, where the smuon and stau are almost degenerate. As $\tan\beta$ increases, the LFV width decreases if flavor is only violated in the LL sector, since the lightest stau becomes mostly right-handed. However, in a GUT-inspired model the running of couplings from the Planck to the GUT scale may introduce significant corrections to the right-handed slepton masses, giving in principle rise to the possibility of enhanced rates at large $\tan\beta$ as well. We address these considerations in a more elaborate study of the complete mixing effects.

- *Detailed study of the supersymmetric spectrum and parameter space:* We pay particular attention to regions that lead to large values of $\Gamma(\chi_2 \rightarrow \chi + \tau^\pm + \tau^\mp)$ through on-shell slepton production, $(BR(\chi_2 \rightarrow \chi\tau^\pm\mu^\mp) = \sum_{i=1}^3 [BR(\chi_2 \rightarrow \tilde{l}_i\mu)BR(\tilde{l}_i \rightarrow \tau\chi) + BR(\chi_2 \rightarrow \tilde{l}_i\tau)BR(\tilde{l}_i \rightarrow \mu\chi)])$, while satisfying all phenomenological and cosmological (relic density) constraints. The characteristic parameter region for the signal in the τ channel to be optimal is defined by the following:

- (i) $m_{\chi_2} > m_{\tilde{\tau}} > m_\chi$;
- (ii) we also assume that one of the mass differences in (i) is $> m_\tau$ and the other $> m_\mu$, $m_{\tilde{\tau}} > m_\chi$, so that the μ, τ and $\tilde{\tau}$ are all on-shell;
- (iii) Moderate values of m_χ (phase space and luminosity considerations).

These conditions are obeyed in significant fractions of the stau coannihilation region.

- *PYTHIA event simulation:* We use PYTHIA to simulate the hadronic decays of τ s produced in the dilepton decay of the second-lightest neutralino, $\chi_2^0 \rightarrow \tilde{l}l \rightarrow \chi ll$ [8]. In the study of the flavor-violating dilepton signal ($\tau^\pm\mu^\mp$), the second lepton is tagged as a muon with a probability equal to the branching ratio assumed for flavor-violating decays.

After first setting the theoretical scene, our procedure in this paper is a bottom-up one, namely:

- (i) Knowing what branching ratio would be required for an observable signal at the LHC, through an event simulation performed using PYTHIA;
- (ii) We study the theoretical frameworks that may satisfy the conditions for observability, together with the supersymmetric parameter space requirements. In doing so, we review look

at models with mixing arising mainly in the left-handed slepton sector, which could not produce an observable signal, and then discuss the possibility of mixing in the right-handed sector, which becomes possible in non-minimal GUTs, where effects due to renormalization above M_{GUT} schemes may become relevant.

The structure of our paper is as follows. Different theoretical frameworks are reviewed in Section 2, the supersymmetric parameter space is explored in Section 3, our simulation is described in Section 4 and its results in Section 5. Our conclusions are summarized in Section 6.

2 Possible Sources of Charged-Lepton Flavour Violation

2.1 Renormalization below M_{GUT}

In the minimal supersymmetric extension of the seesaw mechanism for generating neutrino masses with three heavy singlet-neutrino states N_i , the leptonic sector of the superpotential is:

$$W = N_i^c (Y_\nu)_{ij} L_j H_2 - E_i^c (Y_e)_{ij} L_j H_1 + \frac{1}{2} N_i^c \mathcal{M}_{ij} N_j^c + \mu H_2 H_1, \quad (1)$$

where Y_ν is the neutrino Dirac Yukawa coupling matrix, \mathcal{M}_{ij} is the Majorana mass matrix for the N_i , the L_j and H_I are lepton and Higgs doublets, and the E_i^c are singlet charged-lepton supermultiplets. The superpotential of the effective low-energy theory, obtained after the decoupling of heavy neutrinos is [10]

$$W_{eff} = L_i H_2 \left(Y_\nu^T (\mathcal{M}^D)^{-1} Y_\nu \right)_{ij} L_j H_2 - E_i^c (Y_e)_{ij} L_j H_1. \quad (2)$$

In the basis where the charged leptons and the heavy neutrino mass matrices are diagonal, one finds

$$\mathcal{M}_\nu = Y_\nu^T (\mathcal{M}^D)^{-1} Y_\nu v^2 \sin^2 \beta, \quad (3)$$

where $v = 174$ GeV and $\tan \beta \equiv v_2/v_1$.

In the context of the CMSSM, the soft supersymmetry-breaking masses of the charged and neutral sleptons are assumed to be universal at the GUT scale, with a common value m_0 . In the leading-logarithmic approximation, the non-universal renormalization of the soft supersymmetry-breaking scalar masses is given by

$$(m_{\tilde{L}}^2)_{ij} \simeq -\frac{1}{8\pi^2} \left(\lambda_{\nu_3}^2 V_D^{*3i} V_D^{3j} \log \frac{M_{\text{grav}}}{M_{\nu_3}} + \lambda_{\nu_2}^2 V_D^{*2i} V_D^{2j} \log \frac{M_{\text{grav}}}{M_{\nu_2}} \right) (3m_0^2 + a_0^2). \quad (4)$$

implying that the corresponding corrections to left-handed slepton masses are given by V_D , the Dirac neutrino mixing matrix in the basis where the d -quark and charged-lepton masses are diagonal. In this approach, non-universality in the soft supersymmetry-breaking left-slepton

masses is much larger than that in the right-slepton masses, particularly when the trilinear soft supersymmetry-breaking parameter $A_0 = 0$. Consequently, within the CMSSM, to a good approximation, the renormalization of the soft supersymmetry-breaking parameters at low energies can be understood in terms of the dominant non-universality in the third-generation left-slepton mass: $m_{0LL}^2 = \text{diag}(m_0^2, m_0^2, x \times m_0^2)$, where a typical value of the non-universality factor is $x \sim 0.9$. Based on the above, in [9] we assumed that there is an off-diagonal $\tilde{\tau}_L - \tilde{\mu}_L$ mixing term in the soft mass-squared matrix

$$\Delta m_{0LL}^2 \sim (1-x)m_0^2 \frac{\sin(2\phi)}{2}, \quad (5)$$

where ϕ is the mixing angle between the second and third generation in the charged-lepton Yukawa matrix. This mixing leads to lepton-flavour violation $\sim \sin^2(2\phi)$.

In our current work, we go beyond the above approximation by including the complete mixing effects in interesting regions of the parameter space. For the structures of the mixing matrices, as well as the heavy and light neutrino hierarchies, one must appeal to a specific GUT model. Here we consider textures obtained by combining SU(5) with a U(1) family symmetry. Requiring that fields in the same GUT multiplets have the same flavour charge leads straightforwardly to fermion mass matrices of the following forms [11, 12]

$$\mathcal{M}_u \propto \begin{pmatrix} \bar{\epsilon}^6 & \bar{\epsilon}^5 & \bar{\epsilon}^3 \\ \bar{\epsilon}^5 & \bar{\epsilon}^4 & \bar{\epsilon}^2 \\ \bar{\epsilon}^3 & \bar{\epsilon}^2 & 1 \end{pmatrix}, \quad M_{down} \propto \begin{pmatrix} \bar{\epsilon}^4 & \bar{\epsilon}^3 & \bar{\epsilon}^3 \\ \bar{\epsilon}^3 & \bar{\epsilon}^2 & \bar{\epsilon}^2 \\ \bar{\epsilon} & 1 & 1 \end{pmatrix}, \quad M_\ell \propto \begin{pmatrix} \bar{\epsilon}^4 & \bar{\epsilon}^3 & \bar{\epsilon} \\ \bar{\epsilon}^3 & \bar{\epsilon}^2 & 1 \\ \bar{\epsilon}^3 & \bar{\epsilon}^2 & 1 \end{pmatrix}, \quad (6)$$

with $\bar{\epsilon} \sim 0.2$ as the preferred value. The mass structure and the mixings of the neutrinos are more complicated, because of the heavy Majorana masses of the right-handed components arising from terms of the form $\nu_R \nu_R \Sigma$, where Σ is an SU(3) \times SU(2) \times U(1)-invariant Higgs field with $I_W = 0$ and a non-zero flavour U(1) charge. A working example was given in [13]:

$$M_{RR} \propto \begin{bmatrix} \bar{\epsilon}^{|2n_1+\sigma|} & \bar{\epsilon}^{|n_1+n_2+\sigma|} & \bar{\epsilon}^{|n_1+n_3+\sigma|} \\ \bar{\epsilon}^{|n_1+n_2+\sigma|} & \bar{\epsilon}^{|2n_2+\sigma|} & \bar{\epsilon}^{|n_2+n_3+\sigma|} \\ \bar{\epsilon}^{|n_1+n_3+\sigma|} & \bar{\epsilon}^{|n_2+n_3+\sigma|} & \bar{\epsilon}^{|2n_3+\sigma|} \end{bmatrix},$$

$$m_D^\nu \propto \begin{pmatrix} \bar{\epsilon}^{|1\pm n_1|} & \bar{\epsilon}^{|1\pm n_2|} & \bar{\epsilon}^{|1\pm n_3|} \\ \bar{\epsilon}^{|n_1|} & \bar{\epsilon}^{|n_2|} & \bar{\epsilon}^{|n_3|} \\ \bar{\epsilon}^{|n_1|} & \bar{\epsilon}^{|n_2|} & \bar{\epsilon}^{|n_3|} \end{pmatrix}, \quad m_{eff} \propto \begin{pmatrix} \bar{\epsilon}^2 & \bar{\epsilon} & \bar{\epsilon} \\ \bar{\epsilon} & 1 & 1 \\ \bar{\epsilon} & 1 & 1 \end{pmatrix}. \quad (7)$$

Appropriate choices of the unspecified U(1) charges, such as $n_1 = 2, n_2 = -1, n_3 = 1, \sigma = -1$ (where the n_i are the U(1) charges of the right-handed neutrinos, and σ is the U(1) charge of the field Σ) lead to interesting phenomenology.

We use an indicative choice of coefficients for these SU(5) textures given in [13], which is summarised in Table 1 below.

	Parameters in an SU(5) model with large $\tan\beta$
Charged leptons	$a_{12}^e = 0.6, a_{13}^e = 0.9, a_{22}^e = 1.2, a_{23}^e = -0.5e^{i\pi/3}$ $a_{31}^e = 0.7, a_{32}^e = 0.6, a_{33}^e = 0.4$
m_D^ν	$a_{12}^\nu = 1.3, a_{21}^\nu = -1.3, a_{22}^\nu = 0.7$ $a_{23}^\nu = 1.8e^{i\pi/5}, a_{32}^\nu = 0.7, a_{33}^\nu = 0.5$
M_{RR}	$a_{22}^N = 1, a_{33}^N = 1.8$

Table 1: *Choice of coefficients that reproduce the fermion data for an SU(5) model with large $\tan\beta$. Coefficients not listed in the table are set to unity.*

2.2 Renormalization above M_{GUT}

One must also keep in mind that the GUT scale may lie significantly below the scale M_{Grav} at which gravitational effects can no longer be neglected¹. In this case, the renormalization of couplings at scales between M_{Grav} and M_{GUT} may induce significant flavour-violating effects, particularly in the right-handed slepton mixing, which is suppressed in minimal schemes such as that described in the previous subsection. The simplest such example is provided by the minimal supersymmetric SU(5) GUT, where the superpotential contains terms of the form $\bar{E}\bar{U}\bar{H}$ (with \bar{H} being a colour-triplet Higgs field that is expected to have a mass $\sim M_{GUT}$). This gives rise to one-loop diagrams that renormalize the right-handed slepton masses. In the leading-logarithmic approximation, these corrections take the form [14]:

$$(m_{\tilde{e}}^2)_{ij} \simeq -\frac{3}{8\pi^2}\lambda_{u_3}^2 V_U^{3i} V_U^{*3j} (3m_0^2 + a_0^2) \log \frac{M_{grav}}{M_{GUT}}, \quad (8)$$

for $i \neq j$, where V_U denotes the mixing matrix in the corresponding couplings in the basis where the u -quark and charged-lepton masses are diagonal. Similarly, the complete leading-logarithmic renormalization of the A_e terms is given by

$$A_e^{ij} \simeq -\frac{3}{8\pi^2}a_0 \left(\lambda_{e_i} V_D^{*3i} V_D^{3j} \lambda_{\nu_3}^2 \log \frac{M_{grav}}{M_{\nu_3}} + \lambda_{e_i} V_D^{*2i} V_D^{2j} \lambda_{\nu_2}^2 \log \frac{M_{grav}}{M_{\nu_2}} \right. \\ \left. + 3\lambda_{e_j} V_U^{*3j} V_U^{3i} \lambda_{u_3}^2 \log \frac{M_{grav}}{M_{GUT}} \right). \quad (9)$$

For the structure of the mixing matrices $V_{U,D}$, one has to go to a specific GUT model. Within the minimal SU(5) GUT, the d -quark mass matrix is the transpose of the charged-lepton mass matrix, V_D is simply the unit matrix, and V_U is related to the familiar CKM matrix. This mechanism therefore provides relatively little mixing.

¹ M_{Grav} might be identified with either the Planck mass $M_P = 1.2 \times 10^{19}$ GeV or some lower string unification scale $M_{string} \sim 10^{18}$ GeV.

2.3 Non-Minimal GUT Effects

In the minimal SU(5) case, the renormalization would be too small to generate observable mixing for universal initial conditions. However, minimal SU(5) also predicts the unsuccessful relations $m_s = m_\mu$ and $m_d = m_e$. These can be modified by non-renormalizable terms in the effective superpotential, such as the fourth-order term $\mathbf{10} - \mathbf{24} - \bar{\mathbf{5}} - \bar{H}$, which make different contributions to the d -quark and charged-lepton mass matrices [15], such as:

$$\lambda(\mathbf{10} - \bar{\mathbf{5}} - \bar{H}) + \lambda'(\bar{H} - \mathbf{10} - \mathbf{24} - \bar{\mathbf{5}}) \rightarrow \lambda\bar{v}(dd^c + e^c e) + \lambda'\bar{v}V(2dd^c - 3e^c e).$$

In this case, in the basis where m_d is diagonal, one has $m_e = m_d^D - 5\lambda'\bar{v}V$, where the matrix of couplings λ' is non-diagonal, in general. The diagonalization of $m_e^D = V_{eR}m_eV_{eL}^+$ then gives $m_e^D = V_{eR}(m_d^D - 5\lambda'\bar{v}V)V_{eL}^+$. Similarly [16], the colour-triplet-induced $e^c u^c$ mixing may receive large corrections for the first two generations. Parametrizing the non-renormalizable correction to this mixing by V_{uR} , the RGE-induced right-slepton mixing is not given by V_{CKM} as in the minimal model, but by the product $V_R = V_{CKM}V_{uR}^+$, where V_{uR} is a potential extra source of right-handed charged-lepton mixing, that can be significantly larger than what is expected in the minimal scheme [15]².

3 Discussion of the Supersymmetric Parameter Space

3.1 First Considerations

In order to identify representative points in the supersymmetric parameter space for which detailed simulations are to be run, we first recall a point considered previously in the literature [8]³. In this work, the following CMSSM point has been studied:

$$\tan\beta = 10, \quad m_0 = 100\text{GeV}, \quad M_{1/2} = 300\text{GeV}, \quad A_0 = 300\text{GeV}. \quad (10)$$

This selection of parameters is displayed as point A in Table 2.

We consider first the effects of flavor-mixing entries on the slepton mass matrices that are introduced to mimic the non-diagonal terms induced in the M_{LL}^2 sector by a generic ‘seesaw’ mechanism:

$$\left(M_{LL}^2\right)_{23} = \delta \cdot \left(M_{LL}^2\right)_{22}, \quad (11)$$

²These non-renormalizable corrections also change the forms of the fermion mass matrices, and hence the predictions of this type of flavour-texture model within minimal SU(5). Thus, these corrections would also affect the renormalization between the GUT and heavy-neutrino mass scales. Such effects would have supplementary effects on the the left-handed slepton mixing, but the detailed study of those effects goes beyond the scope of this paper.

³This point is now excluded by the LEP bound on the Higgs mass. Nominally, $m_h > 114.4$ GeV, but we consider supersymmetric points with m_h as low as 111 GeV to be acceptable, so as to make a suitable allowance for uncertainties in the theoretical calculation of m_h .

<i>Point</i>	<i>Modeltype</i>	m_0	$M_{1/2}$	$\tan\beta$	A_0	N_{events}	σ_{int}	L_{int}
A	CMSSM	100	300	10	300	757K	25.3 pb	30 fb ⁻¹
B	SU(5)	40	450	35	40	730 K	2.44 pb	300 fb ⁻¹
C	CMSSM	220	500	35	220	536 K	1.79 pb	300 fb ⁻¹

Table 2: *Parameters of the two reference points A and B (masses in GeV). We also quote the numbers of events simulated, the LHC cross sections and the assumed sample luminosities. Point A is a CMSSM model with universal soft supersymmetry-breaking terms at the GUT scale. Point B is a model with universality assumed at a scale $2 \cdot 10^{17}$ GeV; for comparison with this point, we also present point C, a set of CMSSM parameters that leads to a similar sparticle spectrum and satisfies all the cosmological and phenomenological bounds. In all cases, we work with $\mu > 0$.*

<i>Point</i>	$M_{\tilde{g}}$	$M_{\tilde{u}_L}$	$M_{\tilde{d}_L}$	$M_{\tilde{\chi}_2^0}$	$M_{\tilde{\tau}_1}$	$M_{\tilde{\chi}_1^0}$	$M_{\tilde{l}_R}$	$M_{\tilde{l}_L}$	M_h
A	720	664	669	216	150	118	155	232	110
B	1095	1025	1024	366	207	194	286	371	117
C	1154	1074	1078	388	219	206	290	405	116

Table 3: *Relevant sparticle masses (in GeV) for the reference points defined in Table 2.*

including all the contributing on-shell sfermion exchange diagrams, as given in [17]:

$$BR(\chi_2 \rightarrow \chi\tau^\pm\mu^\mp) = \sum_{i=1}^3 \left[BR(\chi_2 \rightarrow \tilde{l}_i\mu)BR(\tilde{l}_i \rightarrow \tau\chi) + BR(\chi_2 \rightarrow \tilde{l}_i\tau)BR(\tilde{l}_i \rightarrow \mu\chi) \right]. \quad (12)$$

We present in the left panel of Fig. 1 the ratio of the flavor-violating decay width $\Gamma(\chi_2 \rightarrow \chi + \tau^\pm + \mu^\mp)$ to the CMSSM flavor-conserving decay width $\Gamma(\chi_2 \rightarrow \chi + \tau^\pm + \tau^\mp)$ for $\delta = 0$. We find similar values to those in [8], where only the dominant $\tilde{\tau}_1$ exchange diagram was included.

As shown later, in order to have significant LFV signals, we need $\Gamma(\chi_2 \rightarrow \chi + \tau^\pm + \mu^\mp)/\Gamma(\chi_2 \rightarrow \chi + \tau^\pm + \tau^\mp) \sim 0.1$. We see in the left panel of Fig. 1 that this ratio corresponds to $\delta \sim 0.25$. However, a potential problem for such points arises from $BR(\tau \rightarrow \mu\gamma)$, which tends to become too large. This is shown in the right panel of Fig. 1, in which typical values are much larger than the estimated value of $BR(\tau \rightarrow \mu\gamma) \sim 10^{-9}$ in [8]. We recall that the current experimental upper bound is $< 6.8 \cdot 10^{-8}$ [18].

When a similar choice of CMSSM parameters is considered in the framework of an SU(5) model with seesaw neutrinos like the one described in Sections 3 and 4 we find that by setting $M_R = 3 \cdot 10^{14}$ GeV we obtain a value of $\delta \sim 0.05$ leading to a prediction $BR(\tau \rightarrow \mu\gamma) \sim 3 \cdot 10^{-8}$. This would be acceptable for $\tau \rightarrow \mu\gamma$, but would not lead to observable $\chi_2 \rightarrow \chi + \tau^\pm + \mu^\mp$ decay. Due to the strong bound imposed by $\tau \rightarrow \mu\gamma$, it is very difficult to obtain reasonable values of δ using only the LL mixing found in seesaw models.

However, mixing in the RR sector can enhance the decays so that they might be detectable

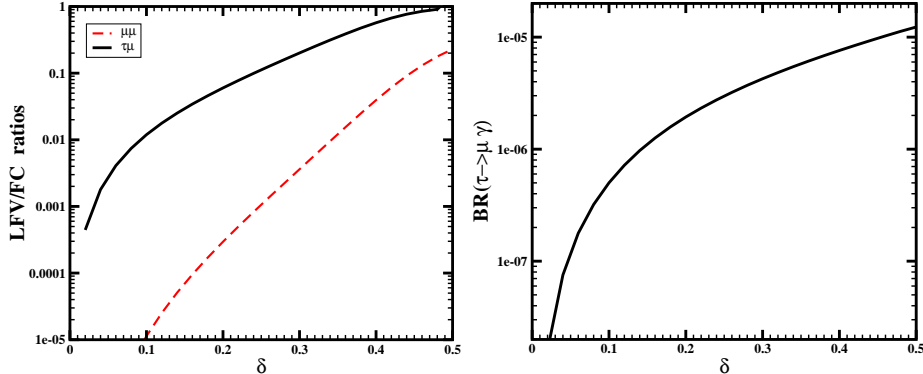


Figure 1: In the left panel, flavor-conserving and -violating dilepton branching ratios are calculated for point A, for comparison with Fig. 1 of [8]. The corresponding expectations for $\tau \rightarrow \mu\gamma$ decay are shown in the right panel as a function of δ .

at the LHC without a large increase in $BR(\tau \rightarrow \mu\gamma)$, since RR mixing enters only in the subdominant one-loop neutralino-exchange diagram for this process. It is considerably smaller than the dominant chargino-exchange diagram for this process, which is sensitive to LL mixing. However, as we have already discussed, significant mixing in the RR sector of the slepton mass matrix cannot be obtained in minimal SU(5) with the conventional seesaw mechanism, but may be obtained in more general GUT scenarios ⁴

In order to see how a branching ratio for $\chi_2 \rightarrow \chi + \tau^\pm + \mu^\mp$ decay that could be observable at the LHC might be induced by non-diagonal entries in the M_{RR} sector of the charged-slepton mass matrix, without violating the $\tau \rightarrow \mu\gamma$ bound, we parametrize as follows the LFV entries in the charged-slepton mass matrices:

$$\begin{aligned} (M_{LL}^2)_{23} &= \delta_{LL} \cdot (M_{LL}^2)_{22}, \\ (M_{RR}^2)_{23} &= \delta_{RR} \cdot (M_{RR}^2)_{22}. \end{aligned} \quad (13)$$

We illustrate in Fig. 2 the different dependences of the branching ratios for $\chi_2 \rightarrow \chi + \tau^\pm + \mu^\mp$ and $\tau \rightarrow \mu\gamma$ decays on the magnitudes of the off-diagonal LL and RR LFV mixing entries.

The upper plots in Fig. 2 display the dependences of the $\chi_2 \rightarrow \chi + \tau^\pm + \mu^\mp$ decays of interest, and the lower plots display the dependences of the branching ratio for $\tau \rightarrow \mu\gamma$ decay. The left plots show the dependences on δ_{LL} for certain discrete choices of δ_{RR} , and the roles of LL and RR mixing are reversed in the right plots. We see again that if RR mixing were negligible a 10% ratio of the LFV $\chi_2 \rightarrow \chi + \tau^\pm + \mu^\mp$ decays relative to the flavour-conserving ones would require large LL mixing with $\delta_{LL} \sim 0.25$, which would inevitably imply a violation of the $BR(\tau \rightarrow \mu\gamma)$ bound. On the other hand, we see that a value of $\delta_{RR} \sim 0.02 - 0.03$ would lead to a similar ratio for $\chi_2 \rightarrow \chi + \tau^\pm + \mu^\mp$ decay, whatever the value of δ_{LL} , whilst the LFV radiative tau decay

⁴Large mixing in the RR sector was also found to be necessary for flavour-violating effects to be observable via non-universality in leptonic kaon decays [15].

could remain within the acceptable experimental range if δ_{LL} were below about 0.03. We also observe that the size of δ_{RR} required to obtain the desired ratios increases as $\tan\beta$ increases, requiring physics beyond the minimal SU(5) model, as discussed in Section 2.3.

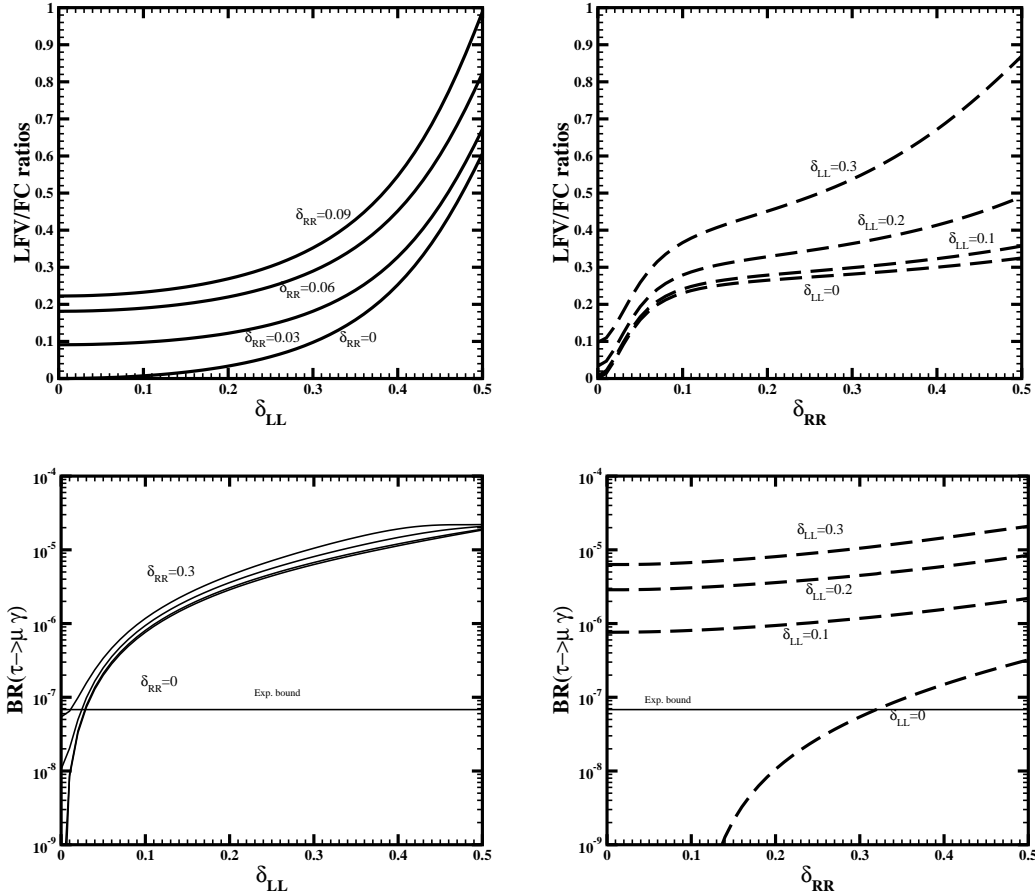


Figure 2: Branching ratios for point A for $\chi_2 \rightarrow \chi + \tau^\pm + \mu^\mp$ decay (upper plots) and $\tau \rightarrow \mu \gamma$ (lower plots) as functions of δ_{LL} (left) and δ_{RR} (right) for certain discrete choices of δ_{RR} (left) and δ_{LL} (right), for the same CMSSM inputs as in Fig. 1.

3.2 Phenomenological and Cosmological Constraints

The parameter point A discussed in the previous section predicts a neutralino relic density that exceeds the WMAP upper bound, and also predicts $m_h < 111$ GeV, below even the more conservative LEP bound on the Higgs mass allowing for theoretical uncertainties. In this subsection we specify a model that satisfies these phenomenological constraints, and may also incorporate the non-minimal SU(5) GUT model with a seesaw mechanism described earlier.

We assume universal soft supersymmetry breaking at a scale $M_X = 2 \cdot 10^{17}$ GeV $> M_{GUT}$, in which case we find a minimum value of $\tan\beta \sim 31$ for $\mu > 0$, above which $\tilde{\tau} - \chi$ coannihilations

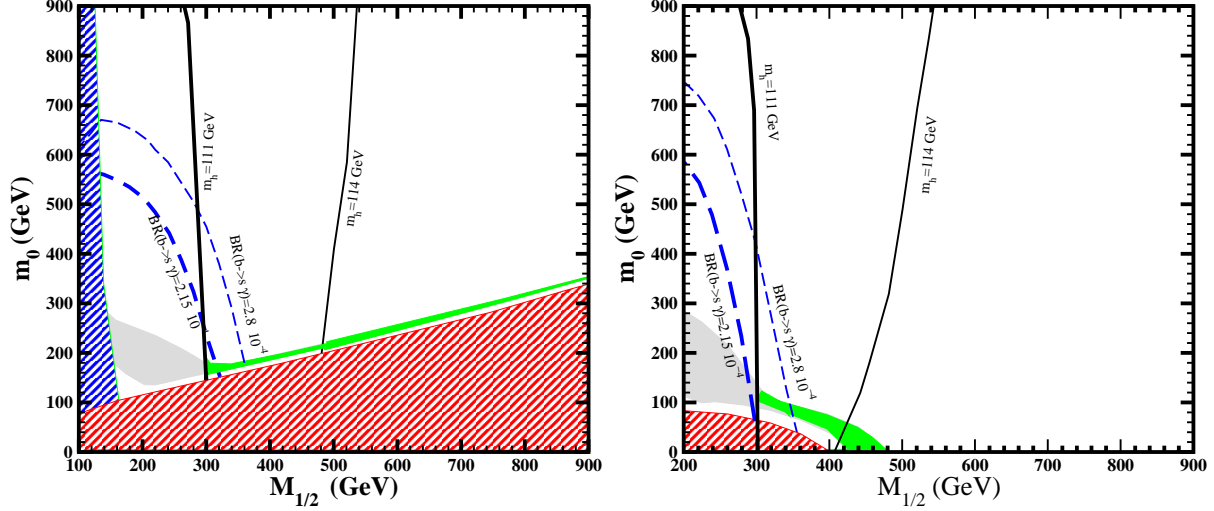


Figure 3: *Cosmologically-favored areas (green) in the $(M_{1/2}, m_0)$ plane for $\tan\beta = 35$ and $A_0 = m_0$, assuming $SU(5)$ unification. In the left panel we assume universality at $M_X = M_{GUT}$, whereas in the right panel we assume universality at $M_X = 2 \cdot 10^{17}$ GeV. The red areas are excluded because $m_\chi > m_{\bar{\tau}}$. We also display the contours for $m_h = 111, 114$ GeV (black solid and thin solid) and $BR(b \rightarrow s\gamma) \cdot 10^4 < 2.15, 2.85$ (blue dashed and thin dashed).*

are sufficient to bring $\Omega_\chi h^2$ below the upper WMAP bound [19]. Furthermore, we find that a minimum value $\tan\beta \sim 35$ is needed to ensure $m_h > 114$ GeV, though we recall that we assign a theoretical uncertainty of ~ 3 GeV to the theoretical calculation of m_h . The GUT Yukawa coupling relation $Y_\tau = Y_b$ cannot be achieved for $\mu > 0$ [20] due to the large supersymmetric threshold corrections to m_b . However, lepton mixing effects may modify the GUT relation:

$$Y_b(GUT) = Y_\tau(GUT)(1 - x), \quad (14)$$

where x is a parameter that accounts for a sizeable 2-3 generation mixing in the charged-lepton Yukawa coupling matrix [21, 22, 23].

We display in Fig. 3 two $(M_{1/2}, m_0)$ planes for the same choice $\tan\beta = 35$. In the left panel, we assume universality at $M_X = M_{GUT}$, whereas in the right panel we show the changes in the allowed parameter space when $M_X = 2 \cdot 10^{17}$ GeV. In the latter case, we find a region of parameter space in which the WMAP bound on the cold dark matter density is respected simultaneously with the conservative bound $m_h > 114$ GeV. In both cases, we fix $m_b(M_Z) = 2.92$ GeV, which corresponds to the evolution of the central value of the \overline{MS} value $m_b(mb) = 4.25$ GeV with $\alpha_s(M_Z) = 0.172$. With this choice of m_b , we find a value $x = 0.37$ in (14).

In order to take into account the cosmological and phenomenological considerations discussed above, we now study point B in Table 2, whose sparticle spectrum is tabulated in Table 3. Point A is taken from [8] and is included so as to facilitate comparisons. As we shall see, point B allows for an observable number of events with the luminosity expected at the LHC.

We display in Fig. 4 for point B the same sets of branching ratios as were shown in Fig. 2 for point A. We see in the top panels that in this case we also need large non-diagonal entries

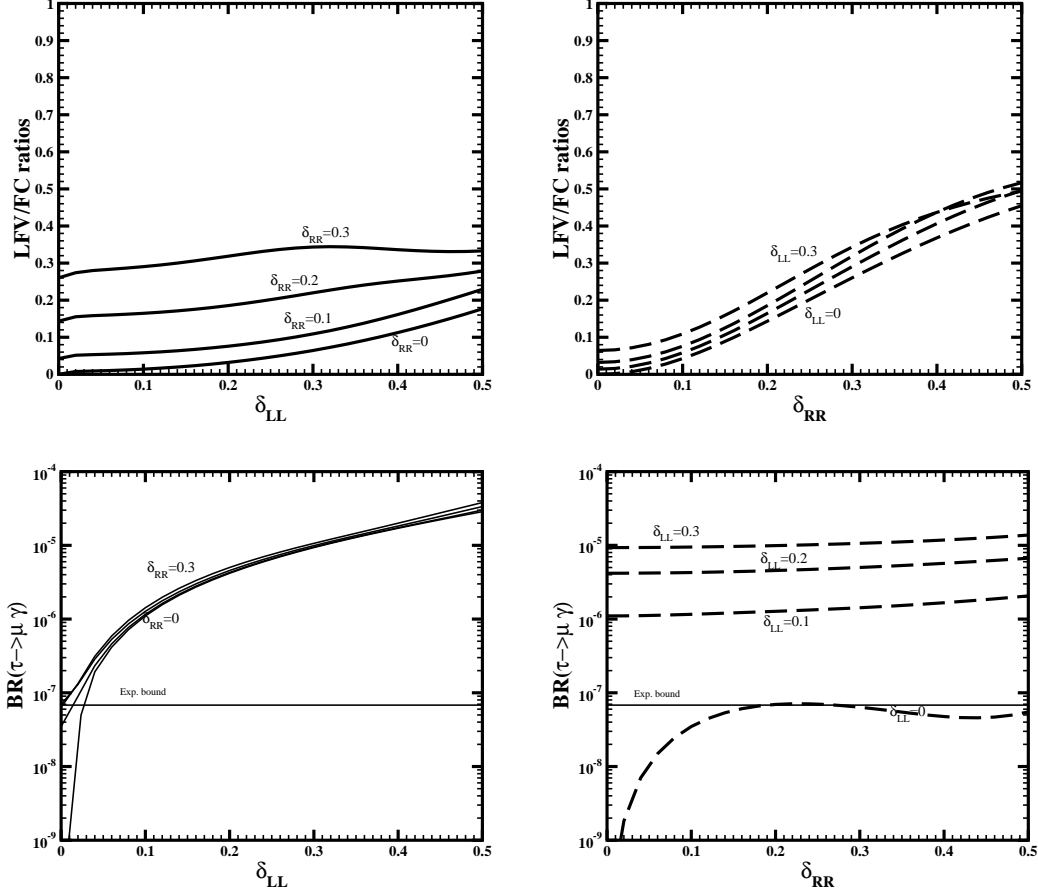


Figure 4: Branching ratios, as in Fig. 2, for the point B described in the text.

in the slepton mass matrix in order to achieve a branching ratio for $\tilde{\chi}_2 \rightarrow \tilde{\chi}_1 \tau^\pm \mu^\mp$ that is of interest for the LHC, e.g., $\delta_{RR} \sim 0.15$ for $\delta_{LL} = 0$ or $\delta_{LL} \sim 0.35$ for $\delta_{RR} = 0$. We also see in the lower panels that $\tau \rightarrow \mu \gamma$ is again very restrictive on the size of δ_{LL} , imposing a maximum value ~ 0.03 . We see in the bottom-right panel that $\delta_{RR} \sim 0.15$ is allowed for $\delta_{LL} = 0$ ⁵. The choice $M_X = 2 \cdot 10^{17}$ GeV opens up the possibility of generating such a value of δ_{RR} though RGE-induced mixing above M_{GUT} . If we assume a generic pattern of non-universal M_{RR}^2 GUT entries of the form:

$$M_{RR}^2(GUT) = \begin{pmatrix} m^2 & 0 & 0 \\ 0 & m^2 & \epsilon \cdot m_0^2 \\ 0 & \epsilon \cdot m_0^2 & m_3^2 \end{pmatrix}, \quad (15)$$

a value $\epsilon \sim 0.25$ is needed to generate the value $\delta_{RR} \sim 0.15$ at the electroweak scale.

⁵If one chose a model with (nominally) the lower value $m_h = 111$ GeV, one could allow lighter masses than for point B, however the limits from $\text{BR}(\tau \rightarrow \mu \gamma)$ on δ_{RR} and δ_{LL} would be more severe.

4 Signals and Backgrounds at the Event Generator Level

This section is devoted to considerations about the detection of LFV in neutralino decays at the LHC, at the event generator level. The signal of tau flavour violation that we consider is an excess of dilepton pairs of the type $\mu\tau_h$ over $e\tau_h$ pairs, where τ_h signifies a hadronic jet produced by hadronic tau decay. The hadronic decay channel for the tau lepton provides a good SUSY signature because: (i) tau leptons decay 65 % of the time to hadrons, and (ii) hadronic jets from tau decays are narrower and have lower particle multiplicity than conventional QCD jets, and they can be reconstructed from the tracking and calorimeter information. Although their charges cannot be determined reliably, tau leptons decaying hadronically can be detected more clearly than taus decaying to lighter leptons because leptons arising from tau decays have two neutrinos, and so are more difficult to reconstruct than leptonic tau decays and separate from background processes.

We present, analyse and compare results from two supersymmetric models with different sparticle spectra, one formulated within the CMSSM and another incorporating additional GUT-inspired physics, as summarized in Tables 2 and 3. The spectra for these points were calculated using ISAJET 7.78 [24] and then interfaced into PYTHIA 6.418 [25], which was used to generate the cross sections, the ensuing QCD parton showers and the hadronic tau decays.

4.1 General Event Cuts

There are some general and distinctive features of R-conserving sparticle production at the LHC. First, the dominant production mechanism is expected to be the pair production of massive squarks and gluinos, which subsequently decay into hadrons, resulting in several hard jets. On the other hand, the neutralino LSP escapes detection and thus we expect large missing transverse energy (MET) in SUSY events. These features suggest using the following definition for the effective mass of the process: $M_{eff} \equiv \cancel{E}_t + p_{t,1} + p_{t,2} + p_{t,3} + p_{t,4}$, where $p_{t,i}$ stand for the transverse momenta of the four hardest jets. The distribution in M_{eff} would exhibit a peak around the scales of the squark and gluino masses.

Keeping these features in mind, we apply the following cuts on the events generated by PYTHIA, for both the SUSY signal and the Standard Model background.

- (i) $N_{jets} \geq 4$ with $p_{T,1} > 100$ GeV and $p_{T,2,3,4} > 50$ GeV,
- (ii) $\cancel{E}_t > 0.2M_{eff}$ and $\cancel{E}_t > \cancel{E}_t^{min}$,
- (iii) $M_{eff} \equiv \cancel{E}_t + p_{T,1} + p_{T,2} + p_{T,3} + p_{T,4} > M_{eff}^{min}$ GeV;

The values of \cancel{E}_t^{min} and M_{eff}^{min} were fixed independently for each set of SUSY parameters, in order to optimize the suppression of the Standard Model background in each case.

4.2 Calorimeter and Object Definition

Only calorimetric smearing and segmentation have been incorporated, since a full detector simulation is out of the scope of the present work. A uniform segmentation $\Delta\phi = \Delta\eta = 0.1$ is assumed and the energy smearing is done according to the following detector parametrization:

$$\begin{aligned} \text{ECAL} &\sim 10\%/\sqrt{E} + 1\%, |\eta| < 3, \\ \text{HCAL} &\sim 50\%/\sqrt{E} + 3\%, |\eta| < 3, \\ \text{FCAL} &\sim 100\%/\sqrt{E} + 7\%, |\eta| > 3. \end{aligned}$$

We use the following object definitions:

- Jets are identified with the help of the PYCELL subroutine of PYTHIA, with $R = 0.4$ used for the jet cone size, due to the high jet multiplicity in SUSY cascade events. We take cells with more than 1 GeV as possible jet triggers and require a sum of $\cancel{E}_T > 10\text{GeV}$ in the calorimeter for the jet to be finally accepted.
- The total missing transverse energy, E_T , is defined as the vector sum of the deposits in the calorimeter cells defined above.
- Leptons are required to be central in rapidity, with $|\eta| < 2.5$, and we use the following isolation demand: no more than 10 GeV of transverse energy should be present in a cone size of $R = 0.2$ around the lepton direction.
- Hadronic tau decays were selected by requiring $p_T > 20$ GeV and $|\eta| < 2.5$, and a ‘matching’ jet with $p_T^{\tilde{\tau}} > 0.8 p_T^{jet}$ and $|\eta| < 2.5$. The jet was tagged as a tau in the two following cases: (i) if the jet-tau distance is no more than $R = 0.4$ in the $\eta - \phi$ plane, or (ii) if the jet-tau distance $R > 0.4$, the jet could also be accepted as a tau, with a probability

$$P = 1 - \left(0.971 p_T^{3/2} - 49\right)^{\frac{5}{3}(1-\epsilon_\tau)} \quad (16)$$

where $\epsilon_\tau = 0.7$ is the selected efficiency.

- Since ISAJET does not allow for LFV decays, flavor-violating dileptons ($\tau^\pm \mu^\mp$) were simulated by counting events with two taus, with at least one of them decaying hadronically; the second tau was then tagged as a muon with a probability equal to the assumed LFV branching ratio (10 %).

4.3 Standard Model Background

Standard Model processes that could in principle contribute to the background for the signature we study here are $t\bar{t}$, WW , QCD jets, Z jets and W jets. The dominant backgrounds

are expected to be $t\bar{t}$ and WW , and only these are considered here. In practice, no event coming from the other processes would satisfy the above-mentioned kinematical requirements when simulated using `PYTHIA`, as used here, and a more extensive study of Standard Model backgrounds is out of the scope of this paper. Such a study would require the use of specialized codes for the evaluation of NLO cross sections and of the exact matrix elements for the parton showers and hadronic decays. The background samples and cross sections used in this work are summarized in Table 4 ⁶.

Process	10 fb ⁻¹	100 fb ⁻¹	σ
$t\bar{t}$	250K	1M	486 pb ⁻¹
WW	250K	1M	70 pb ⁻¹

Table 4: *Standard Model background samples for reference luminosities 10 fb⁻¹ and 100 fb⁻¹, together with their LHC cross sections calculated using `PYTHIA`*

5 Results for LFV at the LHC

In this Section, we analyse the sets of parameters described in Table 2, presenting the results of our event simulations. We recall that point A has been studied previously in [8], and it is included here solely as a consistency check. Point B is based on the SU(5) RGEs in the framework discussed in previous Sections, demanding compatibility with phenomenological and cosmological bounds. We also recall that point C of Table 2 yields a low-energy spectrum and results that are very similar to those of point B.

Plots corresponding to point A (usually placed at the tops of the figure arrays), show the numbers of events normalized to a reference luminosity of 10 fb⁻¹. Plots corresponding to point B (usually placed at the bottoms of the figure arrays) are for an integrated luminosity of 100 fb⁻¹.

5.1 Choices of Cuts

In Fig. 5, we show the M_{eff} and Missing Transverse Energy (MET) distributions of events simulated for point A (top) and point B (bottom).

Plots (a) show the distributions calculated including all the events for both the Standard Model and SUSY, i.e., without applying any of the cuts in (16). We see that the SUSY events exceed

⁶Because the simulations are quite time-consuming, rather than generate the total number of events corresponding to the reference luminosity, we have rescaled the total number of events by an overall factor which, in the case of 100 fb⁻¹, is roughly 2.5 times that for 10 fb⁻¹.

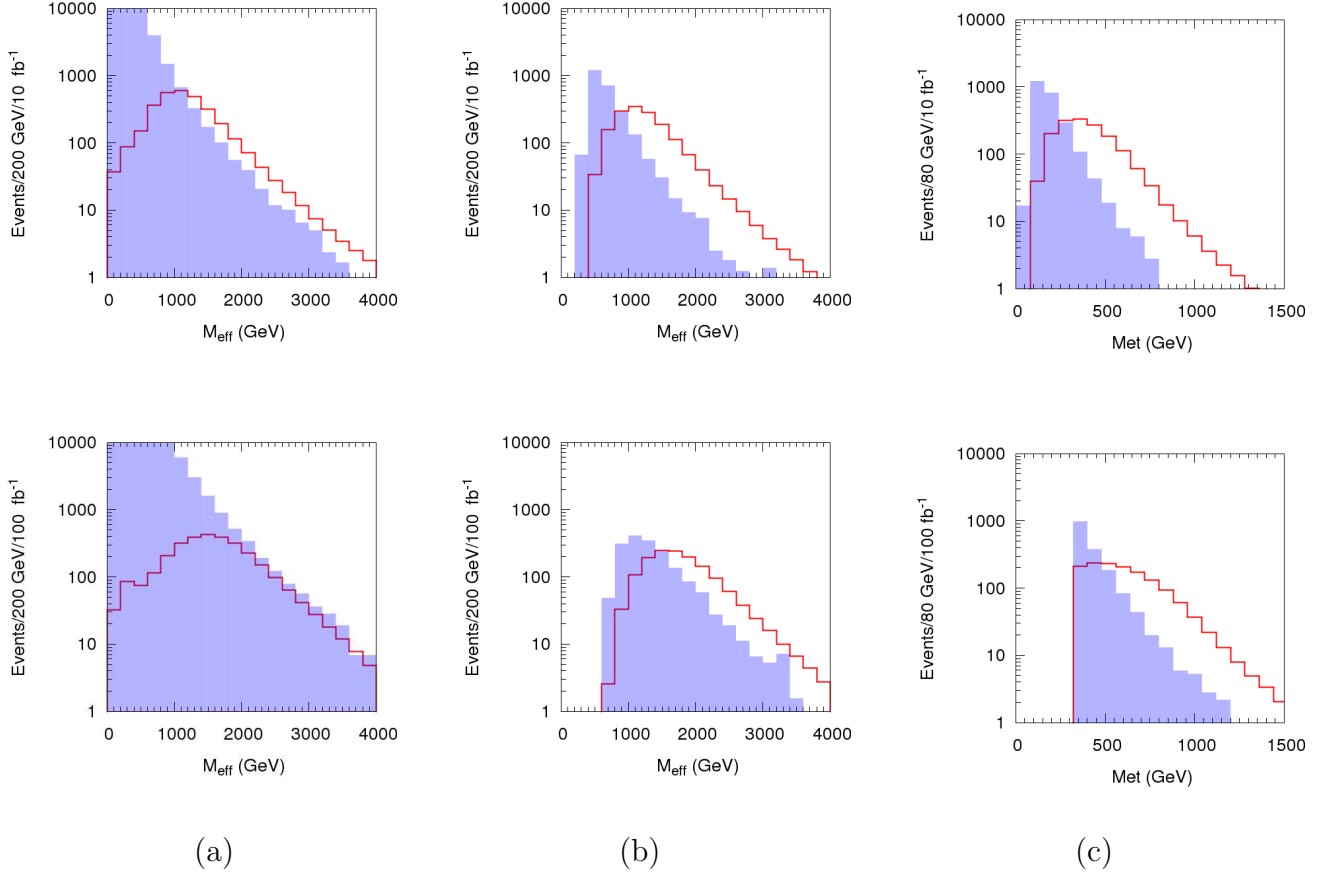


Figure 5: M_{eff} distributions for the crude events (plots a) and after applying cuts (i) and (ii) (plots b), and the Missing Transverse Energy (MET) distributions after applying the same cuts (plots c). The plots on the top correspond to simulations for point A, where $E_t^{min} = 0$; those on the bottom to simulations for point B with $E_t^{min} = 320$ GeV. The signal distributions are shown as (red) solid lines, and the Standard Model backgrounds by the (blue) shaded histograms.

the Standard Model ones at large values of $M_{eff} > 1200$ GeV for point A, whilst the distribution for point B shows larger numbers of Standard Model events than SUSY events over the entire M_{eff} range.

In plots (b), after imposing cuts (i) and (ii) (with $E_t^{min} = 0$ for point A and $E_t^{min} = 320$ GeV for point B), the SUSY events exceed the SM events at ≈ 800 GeV and ≈ 1400 GeV for points A and C respectively. We use these values for M_{eff}^{min} in cut (iii) in the different cases.

Plots (c) show the MET distribution after applying the above cuts. The SUSY event rates exceed those of the Standard Model at energies above ≈ 240 GeV for point A and ≈ 480 GeV for point B. Thus, no cut in MET is needed for point A (it would reduce the Standard Model background but also the SUSY signal, as can be seen below for the invariant mass distributions, which we denote by IMD). However, a cut in MET is required for point B, reducing the total number of accepted SUSY events for point B relative to point A.

5.2 Invariant Mass Distributions

In Fig. 6 we show (left) dilepton IMDs for light leptons and (right) hadronically-decaying τ leptons after imposing the cuts explained in (16), as fixed in the previous subsection 5.1. In the case of point A (top plots), both the opposite-sign same-flavour (OSSF) light dileptons (left) and $\tau^\pm - \tau^\mp$ distributions (right), both shown as red solid lines, exhibit breaks at the characteristic end-points ⁷, which occur at the invariant mass

$$M_l^{max} = \sqrt{\frac{(M_{\tilde{\chi}_2^0}^2 - M_l^2)(M_l^2 - M_{\tilde{\chi}_1^0}^2)}{M_l^2}} = 98.3 \text{ GeV}. \quad (17)$$

On the other hand, the opposite-sign different-flavor (OSDF) (left) and the same-sign $\tau_h^\pm \tau_h^\pm$ distributions (right) do not display such a kinematical constraint. For point B (lower plots) the OSSF end-point does not exist in the light lepton case, and the peak at M_Z is completely obscured by the Standard Model background. In the OS $\tau - \tau$ case, the end-point is at 108.3 GeV.

5.3 Lepton-Flavour-Violating Events

The left plots of Fig. 7 show the visible mass distributions for pairs of hadronically-decaying taus. Excesses of OS pairs (red solid lines) over the SS pairs (green dashed lines) ending approximately at the kinematic end-points can be seen. The structures of the end-points are not as clean as in Fig. 6, because of the energy carried away by neutrinos. In the right plots, an excess of OS $l^\mp \tau_h^\pm$ pairs over the SS pairs can be seen. The distributions of OS LFV $\mu\tau$ pairs (that cannot be distinguished experimentally from $l^\mp \tau_h^\pm$) are also shown for the sake of comparison. In view of the difficulty in distinguishing experimentally the LFV $\mu - \tau$ signal pairs from the Standard Model background, we simulate and plot the excess of $\mu - \tau$ pairs over $e - \tau$ pairs. These should be identical in the Standard Model on average, so any excess of $\mu - \tau$ pairs beyond statistical fluctuations would be a signal of LFV.

In fig. 8 (left) the excesses of $\mu^\mp \tau_h^\pm$ over $e^\mp \tau_h^\pm$ pairs for points A and B are shown. The observable numbers, $N_{\mu\tau_h}^{lfv}$, of $\mu^\mp \tau_h^\pm$ LFV pairs are obtained by summing the counts in the subtracted $\mu^\mp \tau_h^\pm - e^\mp \tau_h^\pm$ distributions in the interval of $M_{l\tau}$ masses between 30 and 110 GeV. We obtain

$$\begin{aligned} \text{Point A : } N_{\mu\tau_h}^{lfv} &= 470 \pm 39 \text{ (12 } \sigma) \\ \text{Point B : } N_{\mu\tau_h}^{lfv} &= 308 \pm 30 \text{ (10 } \sigma) \end{aligned} \quad (18)$$

where we quote only the statistical errors for the signal samples. If we estimate an efficiency of 70 % for the jet-tau matching, a lower number of $(\mu\tau_h)_{lfv}$ pairs would be obtained:

⁷However, the solid curve in the top right panel of Fig. 6 is not observable, since the energy carried off by the ν_τ would escape detection.

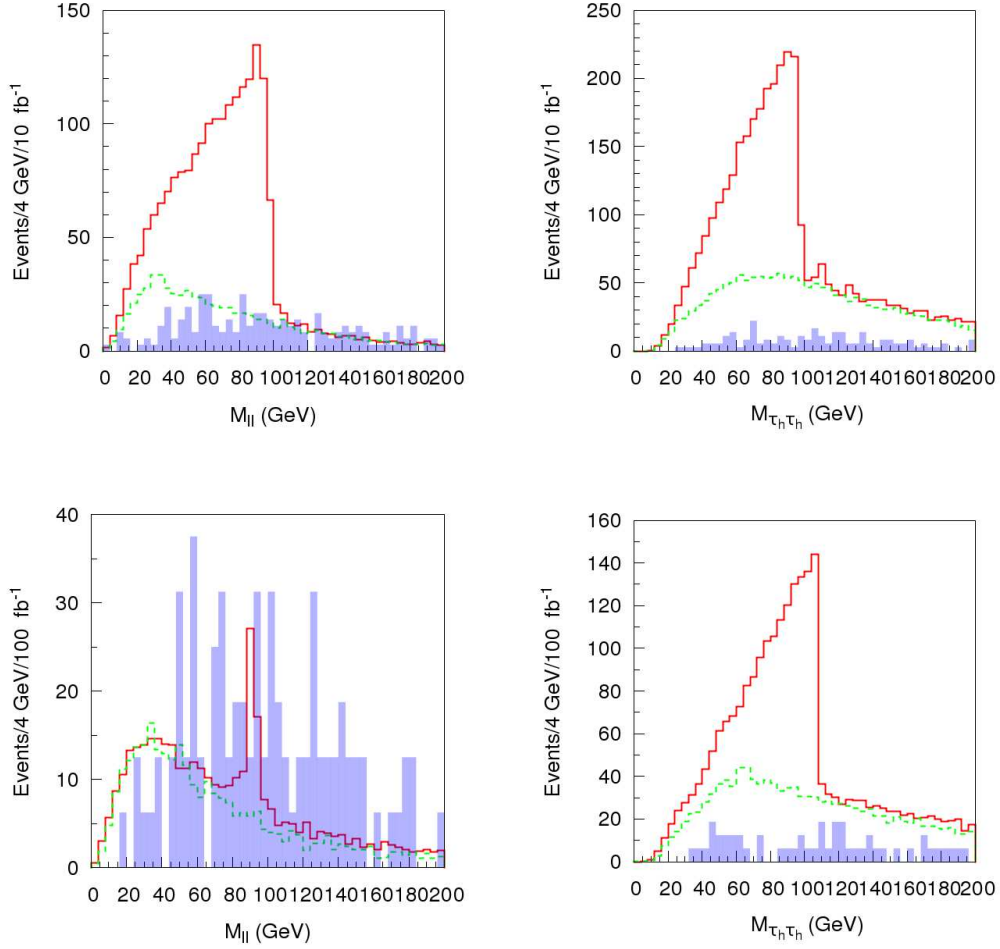


Figure 6: (Left) Dilepton invariant mass distributions for light leptons: opposite-sign same-flavor (OSSF) (red solid line), opposite-sign different-flavor (OSDF) (green dashed line) and the OSSF Standard Model background (shaded). (Right) Hadronically-decaying ditau mass distributions (including the ν_τ four-momenta) with OS (red solid) and SS (green dashed), and the Standard Model background for OS ditau pairs (shaded). The top plots are for case A, and the bottom plots are for case B.

$$\begin{aligned}
 \text{Point A : } N_{\mu\tau_h}^{lfv} &= 355 \pm 34 (10 \sigma) \\
 \text{Point B : } N_{\mu\tau_h}^{lfv} &= 236 \pm 27 (9 \sigma)
 \end{aligned}
 \tag{19}$$

In fig. 9, the excesses of LFV $\mu\tau_h$ pairs over $e\tau_h$ are shown in comparison with the subtraction of $e\tau_h$ pairs from $\mu\tau_h$ pairs obtained from the simulation of the Standard Model background, for points A (left) and B (right). The non-zero subtracted signals for the Standard Model result from the statistical fluctuations in our simulation. The comparison shows that the statistical

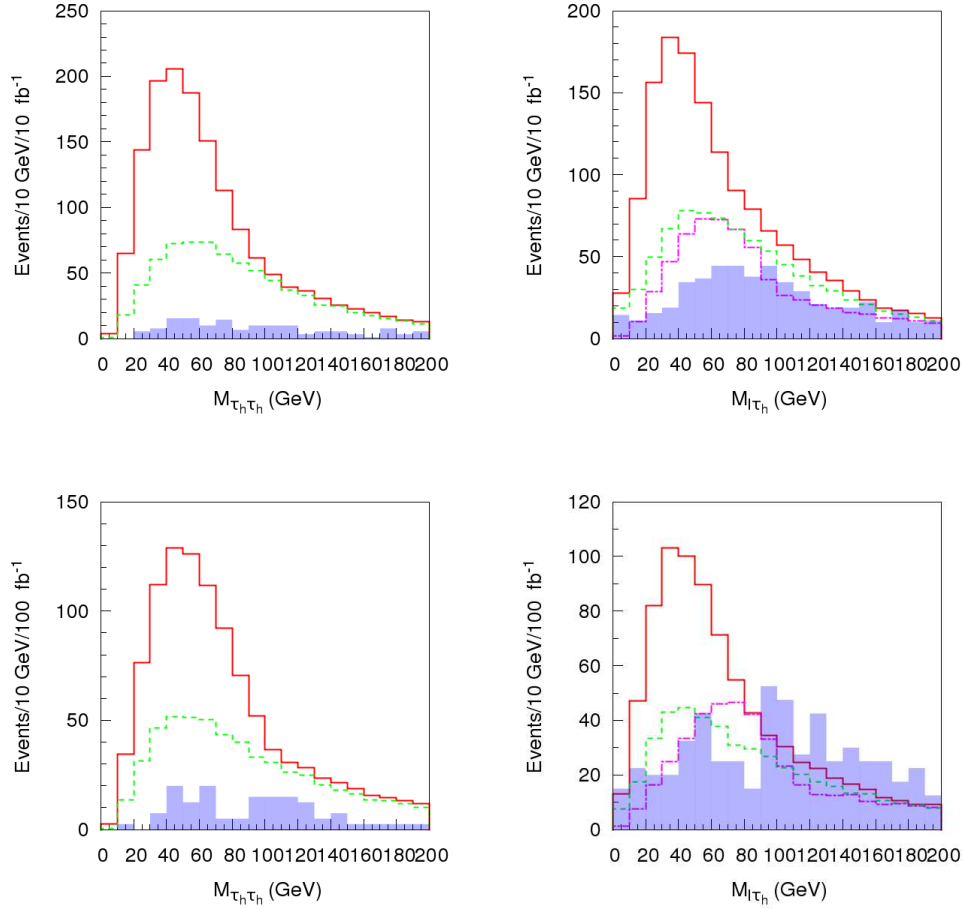


Figure 7: *Left: visible $\tau_h\tau_h$ mass distributions with OS (red solid lines), SS (green dashed lines) and the OS Standard Model backgrounds (shaded). Right: visible $l\tau_h$ mass distributions with OS (red solid lines), SS (green dashed lines), and OS Standard Model backgrounds (shaded). The LFV OS $\mu\tau_h$ pairs are also shown (pink-dot-dashed). As usual, the top plots are for case A and the bottom plots are for case B.*

significance of the LFV signal is quite high in both cases, as it can be separated well from the Standard Model statistical fluctuation: we obtain $S/B \simeq 2.6$ for point B, whilst the ratio is better for point A, namely $S/B \simeq 4.65$.

5.4 Results for Varying m_0 at Fixed $M_{1/2}$

So far, we have restricted our attention essentially to CMSSM points lying in the coannihilation strip where the $\tilde{\tau}_1$ is only slightly heavier than the neutralino LSP, which restricts the kinematics of the τ hadronic jet. Points with the same value of $M_{1/2}$ but larger values of m_0 may also be

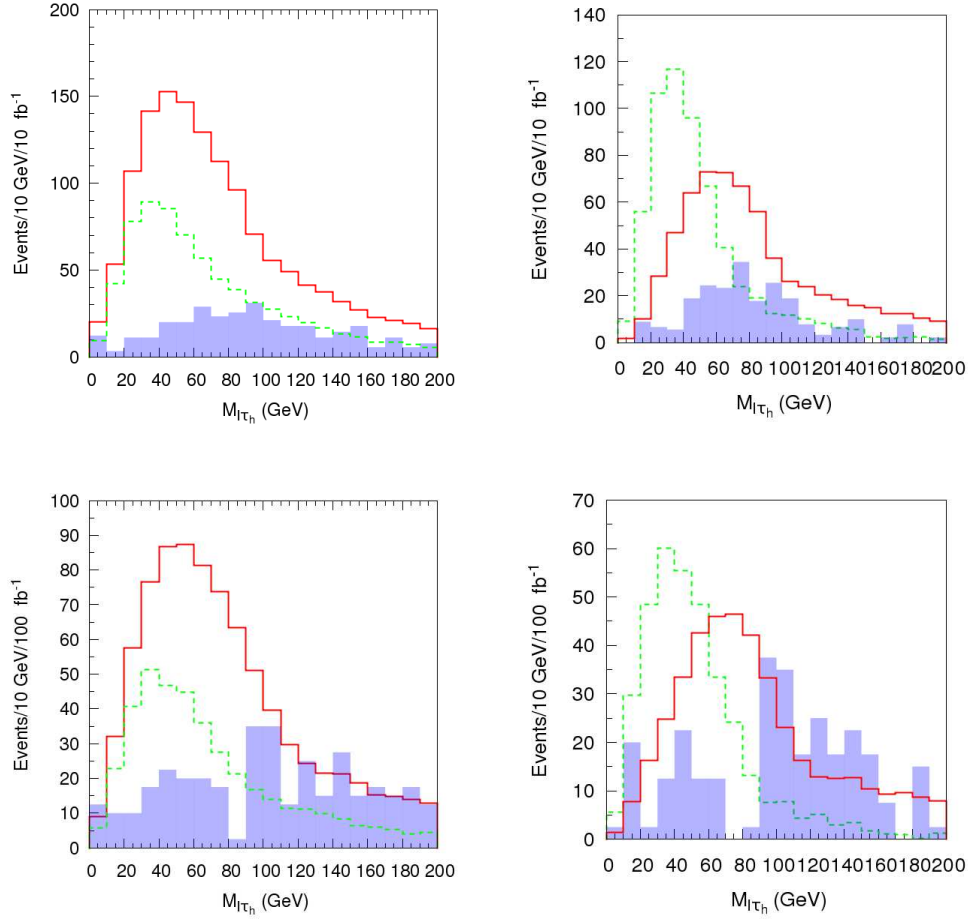


Figure 8: *Left: comparisons between the visible mass distributions for $\tau_h\mu$ (red solid lines), $\tau_h e$ (green dashed lines) and Standard Model $\tau_h\mu$ pairs (shaded). The LFV $\mu\tau_h$ pairs have been added to the $\mu\tau_h$ distribution. Right: comparison between the visible mass distributions for LFV $\mu\tau_h$ (red solid lines), the sign-subtracted distribution $l^\pm\tau_h^\mp - l^\pm\tau_h^\pm$ (green dashed lines), and the sign-subtracted Standard Model backgrounds (shaded).*

allowed under certain circumstances, e.g., in direct-channel resonance regions that may appear at large $\tan\beta$ in the CMSSM or at lower $\tan\beta$ in models with non-universal Higgs masses, or if the gravitino is the LSP. Points with larger m_0 have different kinematics, so here we study the consequences for the observability of LFV in such models. We fix $M_{1/2} = 500$ GeV and $\tan\beta = 35$, and vary m_0 and (slightly) A_0 . We choose four reference points, whose parameters are listed in Table 5, and the resulting sparticle mass spectra in Table 6.

We display in Fig. 10 the numbers of LFV $\mu^\mp\tau_h^\pm$ pairs for each of these points, calculated in the same way as in previous subsection, for the points described in Tables 5 and 6. We also display the statistical error bars. We see that the LFV signal continues to be observable up to the

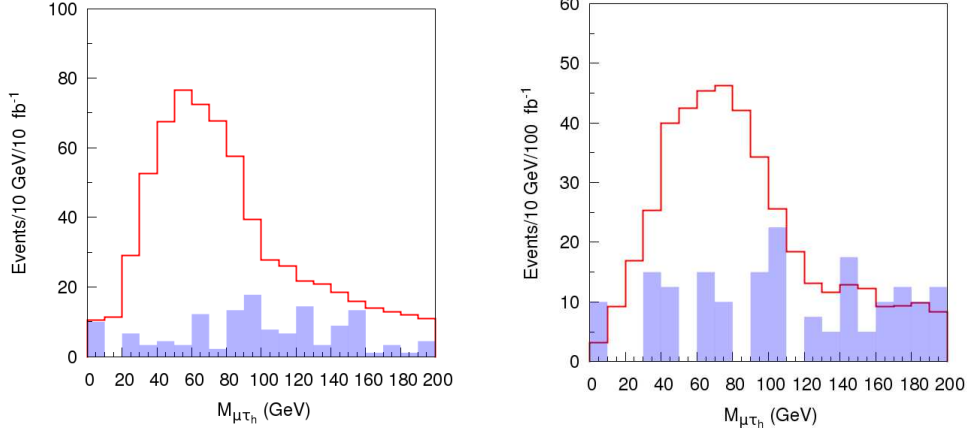


Figure 9: *The signal for excess $\mu\tau_h$ LFV pairs (red solid lines) and subtracted $\mu\tau_h - e\tau_h$ Standard Model backgrounds (shaded) for points A (left) and B (right). As no Standard Model contributions should survive after subtraction, on average, the shaded signals are due to statistical fluctuations.*

Point	m_0	$M_{1/2}$	$\tan\beta$	A_0	N_{events}	σ_{int}	L_{int}
1	250	500	35	250	517K	1.72 pb	300 fb ⁻¹
2	300	500	35	300	494K	1.65 pb	300 fb ⁻¹
3	350	500	35	350	470K	1.57 pb	300 fb ⁻¹
4	400	500	35	400	442K	1.48 pb	300 fb ⁻¹

Table 5: *Parameters of the four CMSSM reference points 1, 2, 3, 4 with increasing values of m_0 and A_0 (all mass parameters are given in GeV units). We also quote the numbers of events, the LHC cross sections and the assumed sample luminosities.*

Point	$M_{\tilde{g}}$	$M_{\tilde{u}_L}$	$M_{\tilde{d}_L}$	$M_{\tilde{\chi}_2^0}$	$M_{\tilde{\tau}_1}$	$M_{\tilde{\chi}_1^0}$	$M_{\tilde{l}_R}$	$M_{\tilde{l}_L}$	M_h
1	1155	1080	1084	388	242	206	314	422	116
2	1157	1092	1095	388	282	206	355	453	115
3	1159	1106	1109	388	323	206	398	487	115
4	1162	1123	1126	388	363	206	442	524	115

Table 6: *Relevant sparticle masses (in GeV) for the reference points defined in Table 5.*

largest value of m_0 studied, namely 400 GeV for point 4 above. We conclude that the analysis described previously in this paper is quite robust, and the LFV signal has a good likelihood of being observable, as long as its branching ratio exceeds about 10%.

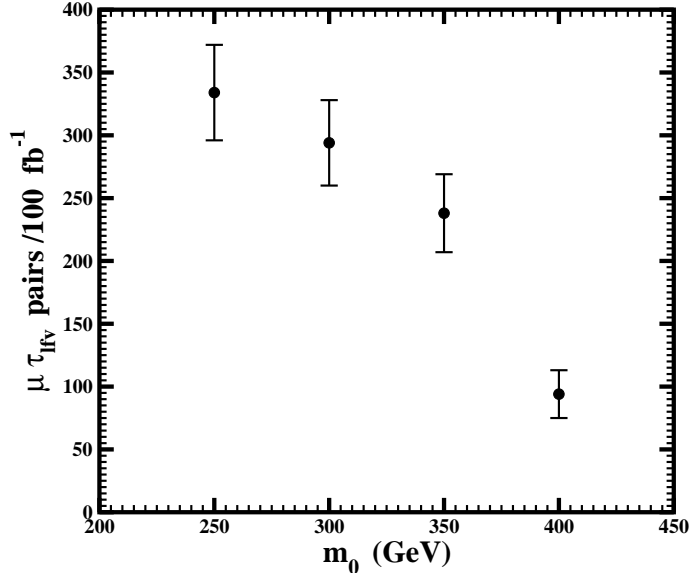


Figure 10: Observable numbers of LFV $\mu^\mp \tau_h^\pm$ pairs for the different points described in Tables 5 and 6, with increasing values of m_0 and A_0 , for fixed $M_{1/2} = 500 \text{ GeV}$ and $\tan \beta = 35$.

6 Conclusions

Motivated by the neutrino oscillation data, and the ensuing likelihood that low-energy violations of charged lepton numbers might be detectable in supersymmetric seesaw models, we have explored the observability at the LHC of sparticle decays that violate τ lepton number. We have worked in the context of the Constrained Minimal Supersymmetric extension of the Standard Model (CMSSM) and in a non-minimal $SU(5)$ GUT extension of the theory. Focusing mainly on regions of the CMSSM parameters with values of the relic neutralino LSP density that fall within the range acceptable to cosmology, we investigate have the SUSY parameter space requirements for tau flavour violation to be observable in $\chi_2 \rightarrow \chi + \tau^\pm \mu^\mp$ decays. We have studied the possible signals from hadronic τ decays, which we have analyzed at the event generator level with the use of PYTHIA.

Within this framework, we have found the following:

- The observation of LFV in neutralino decays at the LHC can be possible if $\Gamma(\chi_2 \rightarrow \chi_1 \tau^\pm \mu^\mp) / \Gamma(\chi_2 \rightarrow \chi_1 \tau^\pm \tau^\mp) \sim 0.1$.
- The strong bounds on radiative τ decays, as well as the other cosmological and phenomenological requirements, constrain significantly the allowed parameter space, to the extent that the CMSSM and the minimal $SU(5)$ GUT are not promising frameworks for observing LFV sparticle decays.
- Larger ratios can be found in a non-minimal $SU(5)$, where RR slepton mixing may be

substantial, enabling the LFV signal to be distinguished clearly from the background.

- The LFV signal remains observable also at larger values of m_0 than are favoured in the usual CMSSM framework.

We conclude that the search for $\chi_2 \rightarrow \chi_1 \tau^\pm \mu^\mp$ decays at the LHC is interesting and complementary to the parallel searches for $\tau \rightarrow \mu \gamma$ decays, and could be a useful ‘canary in the mine’ for non-minimal GUTs.

Acknowledgements

E. Carquin and S. Lola thank the CERN Theory Division and the A.P. Department of the University of Huelva for kind hospitality during several phases of this work. The work of E. Carquin has been partly supported by the MECESUP Chile Grant and the HELEN Program. The work of M.E.G and J.R.Q is supported by the Spanish MEC project FPA2006-13825 and the project P07FQM02962 funded by “Junta de Andalucía”. The research of S. Lola is funded by the FP6 Marie Curie Excellence Grant MEXT-CT-2004-014297.

References

- [1] Y. Fukuda *et al.* [Super-Kamiokande Collaboration], Phys. Rev. Lett. **81** (1998) 1562.
- [2] Y. Fukuda *et al.* [Super-Kamiokande Collaboration], Phys. Rev. Lett. **82** (1999) 1810; Phys. Rev. Lett. **82** (1999) 2430; Q. R. Ahmad *et al.* [SNO Collaboration], Phys. Rev. Lett. **87** (2001) 071301.
- [3] F. Borzumati and A. Masiero, Phys. Rev. Lett. **57** (1986) 961.
- [4] Y. Kuno and Y. Okada, Rev. Mod. Phys. **73** (2001) 151;
- [5] J. Hisano, T. Moroi, K. Tobe and M. Yamaguchi, Phys. Rev. D **53** (1996) 2442; J. Hisano, T. Moroi, K. Tobe and M. Yamaguchi, Phys. Rev. D **53** (1996) 2442; J. Hisano, D. Nomura and T. Yanagida, Phys. Lett. B **437** (1998) 351; W. Buchmüller, D. Delepine and F. Vissani, Phys. Lett. B **459** (1999) 171; M. E. Gómez, G. K. Leontaris, S. Lola and J. D. Vergados, Phys. Rev. D **59** (1999) 116009; J. R. Ellis, M. E. Gómez, G. K. Leontaris, S. Lola and D. V. Nanopoulos, Eur. Phys. J. C **14** (2000) 319; W. Buchmüller, D. Delepine and L. T. Handoko, Nucl. Phys. B **576** (2000) 445; J. L. Feng, Y. Nir and Y. Shadmi, Phys. Rev. D **61** (2000) 113005; J. Sato and K. Tobe, Phys. Rev. D **63** (2001) 116010; J. Hisano and K. Tobe, Phys. Lett. B **510** (2001) 197; S. Baek, T. Goto, Y. Okada and K. Okumura, hep-ph/0104146; S. Lavignac, I. Masina and C.A. Savoy, hep-ph/0106245; D. Carvalho, J. Ellis, M. Gómez and S. Lola, Phys. Lett. B **515** (2001) 323; T. Blazek and S. F. King, hep-ph/0105005.

- [6] N. Arkani-Hamed, H. Cheng, J. L. Feng and L. J. Hall, Phys. Rev. Lett. **77** (1996) 1937; Nucl. Phys. B **505** (1997) 3.
- [7] J. Hisano, M. M. Nojiri, Y. Shimizu and M. Tanaka, Phys. Rev. D **60** (1999) 055008.
- [8] I. Hinchliffe and F. E. Paige, Phys. Rev. D **63** (2001) 115006.
- [9] D.Carvalho, J. Ellis, M. Gomez, S. Lola, J.Romao, Phys. Lett. B **618** (2005) 162.
- [10] For the early works see, e.g., J. Schechter and J. W. Valle, Phys. Rev. D **22** (1980) 2227 and Phys. Rev. D **23** (1981) 1666.
- [11] See, for instance: G. Altarelli and F. Feruglio, Phys. Lett. B **451** (1999) 388.
- [12] S. Lola and G.G. Ross, Nucl. Phys. B **553** (1999) 81.
- [13] J. Ellis, M. Gomez and S. Lola, JHEP **0707** (2007) 052.
- [14] J. Hisano and D. Nomura, Phys. Rev. D **59**, 116005 (1999).
- [15] J. Ellis, S. Lola and M. Raidal, hep-ph/0809.5211.
- [16] J. Hisano, D. Nomura, Y. Okada, Y. Shimizu and M. Tanaka, Phys. Rev. D **58** (1998) 116010.
- [17] A. Bartl, K. Hidaka, K. Hohenwarter-Sodek, T. Kernreiter, W. Majerotto and W. Porod, Eur. Phys. J. C **46** (2006) 783 [arXiv:hep-ph/0510074].
- [18] C. Amsler *et al.* (Particle Data Group), Physics Letters B **667**, 1 (2008)
- [19] L. Calibbi, Y. Mambrini and S. K. Vempati, JHEP **0709** (2007) 081.
- [20] M. E. Gomez, T. Ibrahim, P. Nath and S. Skadhauge, Phys. Rev. D **70** (2004) 035014 [arXiv:hep-ph/0404025].
- [21] G. Leontaris, S. Lola and G.G.Ross, Nucl. Phys. B **454** (1995) 25.
- [22] M. S. Carena, J. R. Ellis, S. Lola and C. E. M. Wagner, Eur. Phys. J. C **12** (2000) 507 [arXiv:hep-ph/9906362].
- [23] M.E. Gomez, S. Lola, P. Naranjo and P. Rodriguez-Quintero, in preparation.
- [24] F. E. Paige, S. D. Protopopescu, H. Baer and X. Tata, arXiv:hep-ph/0312045.
- [25] T. Sjostrand, S. Mrenna and P. Skands, JHEP **05** (2006) 026, (LU TP 06-13, FERMILAB-PUB-06-052-CD-T) [hep-ph/0603175].